(Received 31 October 2024, Accepted 4 December 2024, Scheduled 12 December 2024)

Design and Experimental Study of Dual-Band Left-Handed Filters for Sub-6G Applications

Zhonghui Li, Chen Li, and Minquan Li*

Information Materials and Intelligent Sensing Laboratory of Anhui Province, Anhui University, Hefei 230039, China

ABSTRACT: This paper presents a dual-band microstrip filter with left-handed characteristics, featuring high selectivity and miniaturization. The design achieves negative permittivity and permeability by integrating H-shaped complementary split-ring resonators (CSRRs) within a substrate integrated waveguide (SIW). To enhance out-of-band rejection performance, a defected ground structure (DGS) is introduced. By applying the Half Mode SIW (HMSIW) principle, the equivalent magnetic walls of the SIW are cut, resulting in a 50% size reduction. Dual-frequency characteristics are realized using a symmetrical H-shaped CSRR, with the filter operating in the Sub-6G frequency band. Experimental results demonstrate that the filter exhibits good selectivity and low insertion loss at 3.5 GHz and 4.8 GHz. Tuning of the second frequency band is achieved by adjusting the coupling distance between the CSRR and metal via. This work has significant application potential in the fields of wireless communication and RF technology. The study provides theoretical support and technical insights for the design of future compact multi-band filters.

1. INTRODUCTION

With the growing demand for microwave devices, there has been an increasing focus on filters with enhanced passband performance, including miniaturization, low insertion loss, and multiband capabilities.

Russian scientist Veselago introduced the concept of materials with a negative dielectric constant and magnetic permeability within specific frequency bands. He proposed that these materials, later termed "left-handed materials" or metamaterials, could exhibit unique phenomena such as a negative refractive index and flat plate focusing [1]. British scientist Pendry advanced this field by proposing structural models that could achieve negative permittivity [2] and negative magnetic permeability [3], marking the official beginning of metamaterial research. Falcone et al. studied CSRRs from the perspective of parity and demonstrated their role as metamaterial resonators with negative dielectric properties [4]. This discovery has significantly advanced the study of microwave devices exhibiting left-handed properties. When Split Ring Resonators (SRRs) are combined with rectangular waveguides, they exhibit a stopband when the resonant frequency exceeds the cutoff frequency. If the resonant frequency is below the cutoff frequency, the stopband shifts to a passband. CSRR structures demonstrate a similar behavior and have been applied in the design of microstrip filters [5] and microstrip power dividers [6]. Ref. [7] introduced the use of the resonant mode of the CSRR as a substitute for SIW base mode. By adjusting the size of the CSRR, the SIW band can be effectively controlled, and transmission zeros can be manipulated through the adjustment of metal vias to achieve improved selectivity. In [8], a method was proposed to load two distinct sets of CSRR structures on top of a SIW, allowing independent control of their center frequencies. This design facilitated the creation of a miniaturized filter with high selectivity. In [9], a novel cross-coupled band-pass filter (BPF) based on a new CSRR-SIW resonator was proposed. The Q-factor of the main mode of this resonator was extracted and analyzed, leading to the design of a miniaturized cross-coupled BPF with low insertion loss and improved performance. In [10], a novel dual-band tunable band-pass filter is proposed. This paper introduces for the first time a compact dual-band band-pass filter with a controllable center frequency based on a 90° sector-shaped substrate integrated waveguide resonator (FSSIWR). In [11], it is theoretically and experimentally demonstrated that, over a wide frequency range, the performance of phase modulation links is superior to that of intensity modulation links. In [12], a numerical method is proposed to analyze a new type of notch filter, which is crucial for various applications in telecommunications, sensing, and medical fields.

Unresolved issues regarding filters currently include the following: 1) Miniaturization: As device density becomes a trend, the miniaturization of components has become an important metric for evaluating the quality of a device. 2) Multi-frequency filters: With spectrum resources becoming increasingly scarce, the demand for dual-frequency filters is also rising. 3) Designing filters with simple structures: Filters with complex structures are expensive to manufacture, and some filters with fine lines cannot be produced using current manufacturing techniques, or the error rate is high if they are made. 4) Out-of-band suppression capability: Many existing filter designs exhibit insufficient out-of-band suppression, resulting in inadequate attenuation of signals outside the passband, which adversely impacts the overall signal quality of the system.

* Corresponding author: Minquan Li (AHU411MHz@hotmail.com).

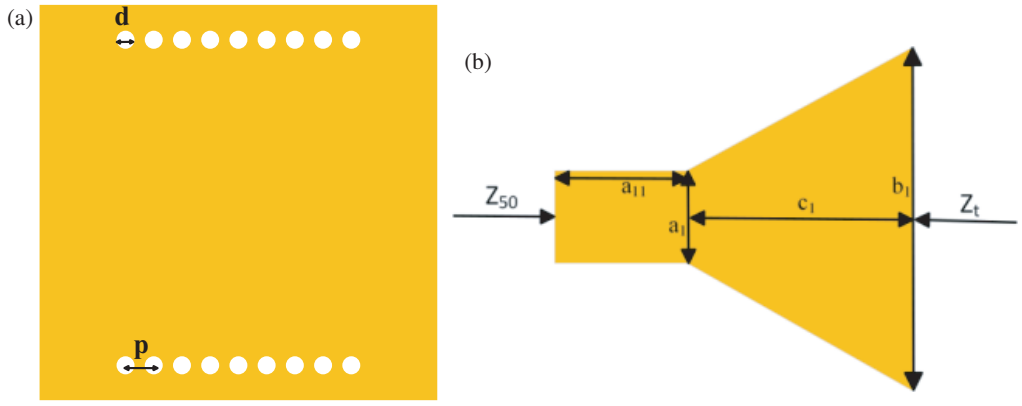

FIGURE 1. (a) The basic structure of SIW. (b) Isosceles trapezoidal transition structure.

The main contributions of this paper are: 1) By cutting the SIW equivalent magnetic wall, the size is reduced by 50% while maintaining high selectivity. 2) Derived the design of a dual-frequency filter from the single-frequency filter design, and developed a tunable frequency dual-frequency filter. 3) On the basis of the single-frequency design, two completely symmetrical H-shaped CSRR structures were etched to achieve dual-frequency transmission characteristics. This was accomplished by adjusting the coupling distance between the CSRR and metal via to control the second frequency band. The designed structure is easy to fabricate. 4) This paper introduces the design of a defected ground structure, which enhances the out-of-band suppression capability of the filter.

A resonant dual-band-pass filter operating in the Sub-6G frequency range was realized by etching H-shaped complementary split-ring resonators on the surface of a substrate-integrated waveguide. A dual-frequency filter based on a half-mode substrate-integrated waveguide was achieved using the equivalent magnetic wall method of cutting SIW filters, reducing the size by 50% without altering the filtering performance. To improve the out-of-band suppression performance of the filter, a defected ground structure was introduced. The presence of the filter's left-handed characteristics was validated through S-parameter inversion. The dimensions of the filter are approximately $0.30\lambda_g \times 0.08\lambda_g$, achieving miniaturization performance.

2. ANALYSIS AND DESIGN

2.1. Analysis of SIW Single-Frequency Filter

Substrate integrated waveguide (SIW) is widely used in various radio frequency (RF) devices due to its low loss, cost effectiveness, and design flexibility. It resembles a conventional rectangular metal waveguide, where two rows of metallic vias arranged in a linear array serve as the equivalent of the waveguide's sidewalls. The cutoff frequency of the SIW, as given in [13], can be expressed as:

$$f_c = \frac{c}{2W_{eff}\sqrt{\varepsilon_r}}, \quad W_{eff} = W_s - \frac{d^2}{0.95s}, \tag{1}$$

where W_s and W_{eff} are the waveguide width and its effective width; c is the speed of light; and ε_r is the substrate dielectric constant. In order to meet the minimum electromagnetic wave leakage, the metal via diameter d and via spacing p should satisfy (2).

$$p > d/2, \quad \frac{p}{\lambda_c} < 0.25, \quad \frac{R}{K_0} < 10^{-4}, \quad \frac{p}{\lambda_c} > 0.06. \tag{2}$$

As shown in Fig. 1(a), p denotes the distance between the via holes, $d/2$ the radius of the metal vias, R the total loss of electromagnetic waves during propagation, K_0 the total wave number of electromagnetic waves propagating in the air, and λ_c the wavelength of electromagnetic waves transmitting in the medium.

The SIW structure shares similarities with rectangular waveguide, but when being integrated with planar structures, it requires a transition design to interface with a microstrip line. To satisfy engineering requirements, the transition structure must be designed with key considerations, including low cost, minimal insertion loss, compact size, and the ability to cover a wide operational bandwidth. This ensures effective integration while maintaining performance and economic feasibility in practical applications. In this paper, an isosceles trapezoidal transition structure is used, as shown in Fig. 1(b). The rectangular section Z_{50} represents the 50 Ω microstrip line, while Z_t is the trapezoidal transition structure for impedance matching between the SIW and microstrip line. a_1 is the width of the 50 Ω microstrip line, b_1 the wide edge of the transition, and c_1 the height of the trapezoidal structure. After calculating Z_t (3) and optimizing the parameters, the final dimensions are $a_1 = 3.5\,\text{mm}$, $b_1 = 11\,\text{mm}$, and $c_1 = 3.0\,\text{mm}$. As shown in Fig. 2(a) and Fig. 2(b), the SIW combined with the transition structure exhibits high-pass transmission characteristics.

$$Z_t = \frac{\pi}{2}\frac{h}{W_{eff,SIW}}\sqrt{\frac{\mu}{\varepsilon}}\frac{1}{\sqrt{1-(\lambda/\lambda_{C,SIW})^2}}. \tag{3}$$

By loading a square CSRR structure with effective low-pass attenuation, a band-pass filter is formed, as illustrated in Fig. 3. The CSRR structure is known for its ability to exhibit negative

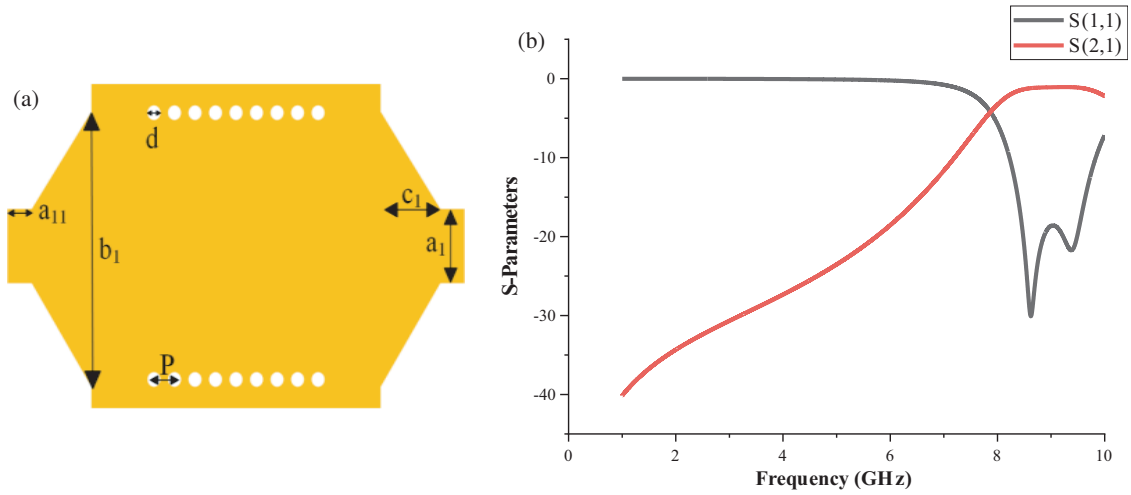

FIGURE 2. (a) SIW combined with trapezoidal transition structure. (b) Simulation results.

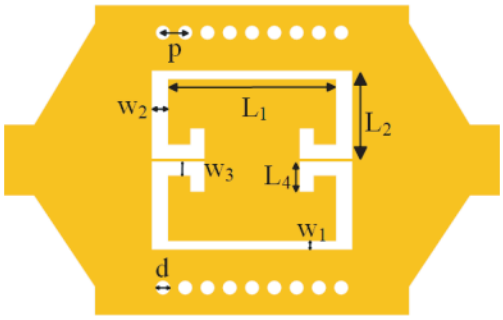

FIGURE 3. SIW loaded conventional CSRR structure filter.

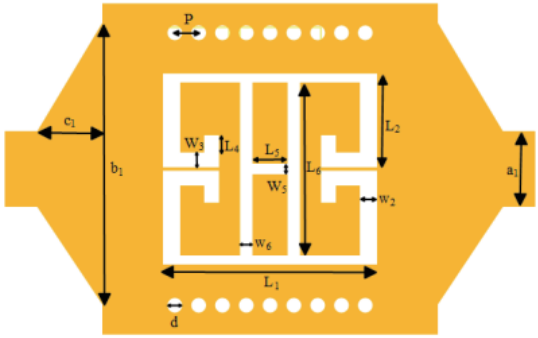

FIGURE 4. SIW loaded H-type CSRR structure filter.

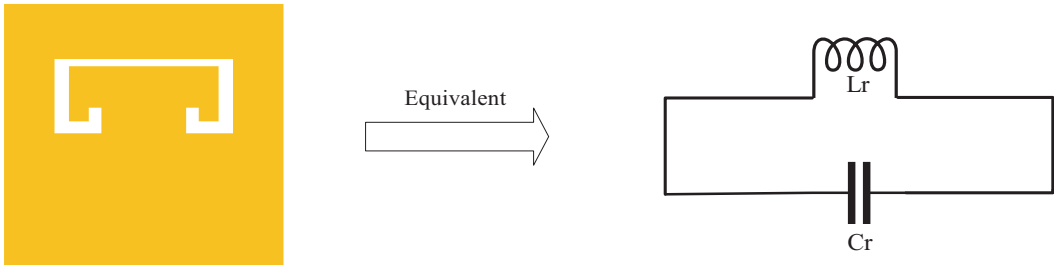

FIGURE 5. Traditional square open resonant ring structure and its equivalent circuit.

permeability, while its complementary structure can generate a negative dielectric constant within the same frequency band. As shown in Fig. 4, loading a conventional square CSRR structure with an H-shaped gap induces negative permeability by blocking most of the transmitted energy, allowing only a small portion to pass. Consequently, the filter designed in this paper, which integrates the SIW with an H-type CSRR structure, exhibits composite right/left handed (CRLH) characteristics.

In this paper, a parallel resonator circuit is employed to model a single-sided C-type open resonant ring, as shown in Fig. 5. The analysis of the newly introduced H-shaped structure will be provided below. Fig. 6 illustrates the H-shaped branch and its equivalent circuit, where C_c represents the gap capacitance along the transverse direction in the H-shaped structure. C_{c1}, C_{c2}, L_{c1}, L_{c2} denote the waveguide transmission lines coupled to the lower and upper slots of the H-shaped slot, respectively. The upper and lower slots in the H-type structure are equivalent to two parallel resonant circuits, namely L_{rs1}, L_{rs2}, C_{rs1}, and C_{rs2}. The H-shaped structure generates a transmission pole, denoted as F_z, which results from the phase difference between the upper and lower paths and is expressed by (4).

$$F_z \approx c/4/\left(l_6/2 - w_6/2\right)/\sqrt{\varepsilon_r}, \tag{4}$$

where c is the speed of light in the vacuum, and ε_r is the relative dielectric constant.

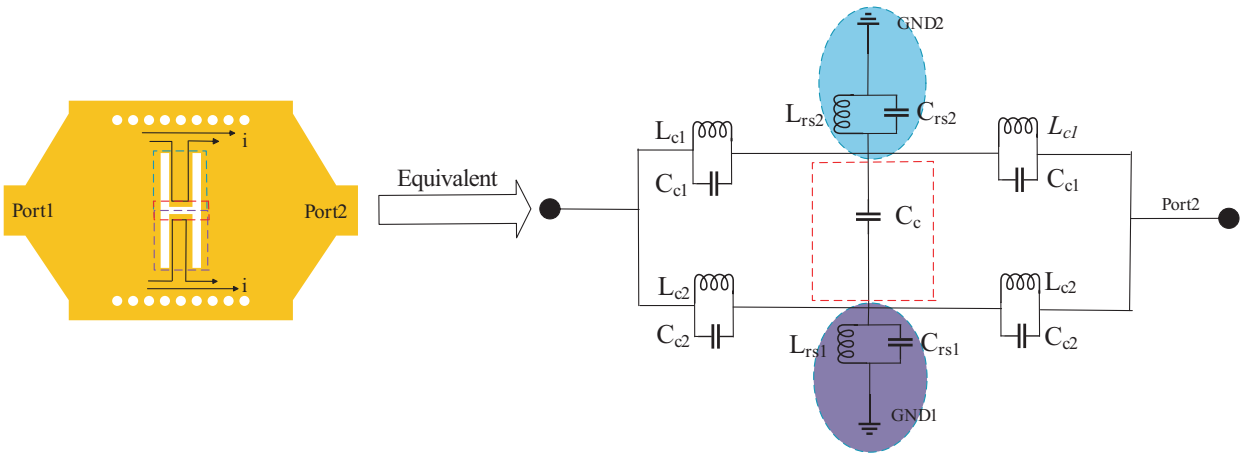

FIGURE 6. H-shaped structure and its equivalent circuit.

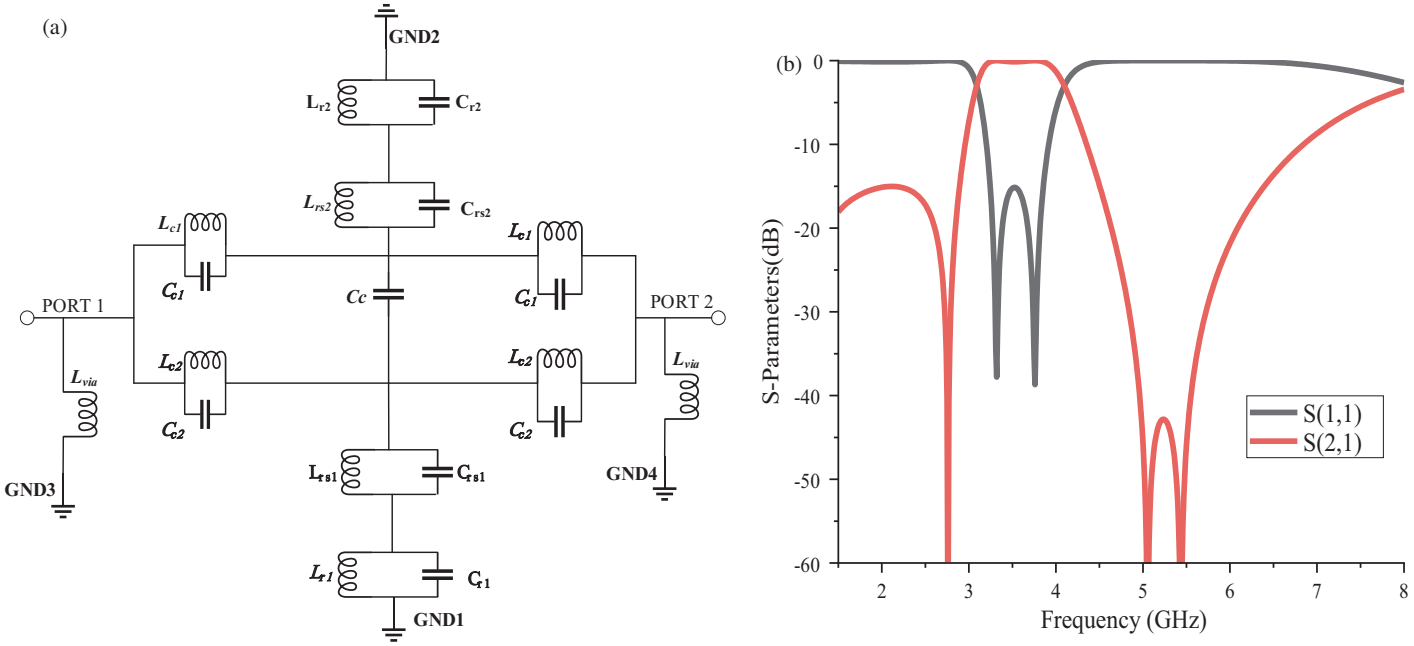

FIGURE 7. (a) SIW loaded H-type CSRR structure equivalent circuit diagram. (b) Simulation results of equivalent circuit diagram.

The equivalent circuit of the H-type CSRR integrated with the SIW is depicted in Fig. 7(a). Here, L_{via} represents the inductance associated with the metal via, while the open resonant ring is modeled by two parallel resonant structures, namely L_{r1}, C_{r1} and L_{r2}, C_{r2}. As shown in Fig. 7(b), after simulating the equivalent circuit using advanced design system (ADS) software and optimizing the circuit parameters, the corresponding electrical values are: $L_{r2} = 2.687$ nH, $C_{r2} = 0.15$ pF, $L_{rs2} = 9.405$ nH, $C_c = 6.44$ pF, $L_{c1} = 1.56$ nH, $C_{c1} = 1.08$ pF, $L_{c2} = 100$ nH, $C_{c2} = 0.361$ pF, $L_{rs1} = 55$ nH, $C_{rs1} = 33.53$ pF, $L_{r1} = 1.472$ nH, $C_{r1} = 0.15$ pF, and $L_{via} = 120$ nH. The simulation results demonstrate the successful design of a single-passband filter with a center frequency of 3.5 GHz, characterized by high selectivity and low insertion loss.

Based on the above theory, this paper chooses to optimize the parameters of the filter using High Frequency Structure Simulator (HFSS) on the dielectric plate of Rogers 5880. The dielectric constant of the plate is 2.2, and the thickness is 1.575 mm. SIW loads the individual parameters of a single H-type CSRR structure filter as follows: $P = 1.1$ mm, $d = 0.7$ mm, $h = 1.575$ mm, $L_1 = 8.3$ mm, $W_1 = 0.42$ mm, $L_2 = 4.35$ mm, $W_2 = 0.82$ mm, $C_1 = 3$ mm, $a_1 = 3.5$ mm, $b_1 = 13$ mm, $W_3 = 0.7$ mm, $W_5 = 0.5$ mm, $L_5 = 2.2$ mm, $L_6 = 8$ mm, $W_6 = 0.59$ mm, $L_4 = 0.8$ mm. Its simulation results can be seen from Fig. 8.

The spacing p of the metal holes primarily affects the in-band performance, so setting an appropriate p value can help reduce the in-band insertion loss of the filter. For the transverse length L_5 of the H-type structure, the equivalent circuit shows that the value of L_5 mainly influences the gap capacitance C_c. As L_5 increases, the equivalent capacitance decreases, causing the frequency to shift toward the high-frequency range. For the

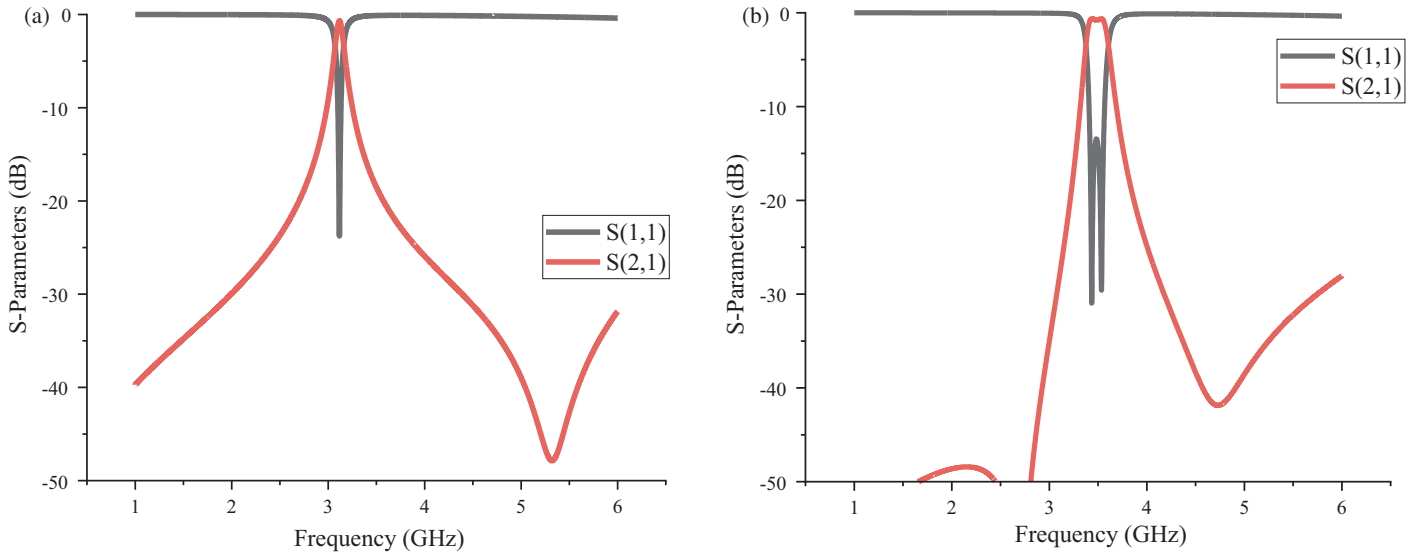

FIGURE 8. (a) Simulation results of SIW loaded conventional square CSRR structure (see Fig. 2). (b) Simulation results of the new CSRR structure of SIW loading H type (see Fig. 3).

longitudinal length L_6 of the H-type structure, it is mainly influenced by the values of L_{rs1}, L_{rs2}, C_{rs1}, and C_{rs2}. When L_6 increases, the corresponding inductance and capacitance values decrease, and the frequency moves toward the high-frequency range.

The simulation results are shown in Fig. 8(b). The maximum insertion loss of this filter is 0.7 dB, and the return loss is less than -15 dB across the entire range. The designed model has dimensions of $0.28\lambda_g \times 0.18\lambda_g$. The passband range is from 3.38 GHz to 3.6 GHz. Clearly, compared to Fig. 8(a), the incorporation of the H-type structure introduces an additional transmission zero around 2.75 GHz. This significantly improves the selectivity of the filter, thereby validating the theoretical principles discussed earlier.

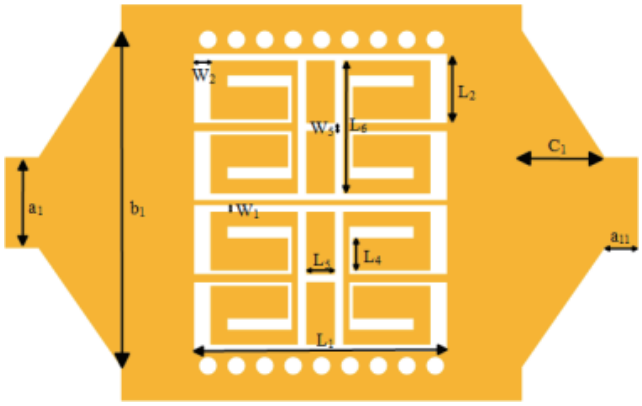

FIGURE 9. SIW loaded filter with symmetrical H-shaped CSRR structure.

2.2. Analysis of SIW Dual-Band Filter

A high-performance single-frequency filter is designed by introducing a single-loaded H-type CSRR structure. To meet the increasing demand for high-performance multi-band filters in communication technology, this paper utilizes a symmetrical H-shaped open resonant ring loaded in the SIW. The coupling effect between the two open resonant rings induces parallel resonance, and by controlling the coupling between the two resonators, the second resonant frequency is tuned to 5.2 GHz. After optimizing the parameters of the CSRR structure, the filter continues to operate at 3.5 GHz, achieving a dual-band filter design. The parameters of the filter, loaded with the new symmetric CSRR structure, are simulated and optimized on a dielectric substrate of the same material thickness. The structure of the proposed filter with the loaded symmetric H-shaped CSRR is shown in Fig. 9.

Based on the analysis of the SIW loaded with the new H-shaped CSRR structure, equivalent circuit model after loading the SIW with the symmetric H-shaped CSRR is shown in Fig. 10, where L_d denotes the coupling inductance between two H-shaped CSRRs, and C_d is the coupling capacitance. L_d and C_d are modeled and optimized using ADS software, and the final optimized electrical parameters are as follows: $L_{r2} = 8.06$ nH, $C_{r2} = 0.15$ pF, $L_{rs2} = 1.609$ nH, $C_c = 3.12$ pF, $L_{c1} = 4.70$ nH, $C_{c1} = 3.55$ pF, $L_{c2} = 320$ nH, $C_{c2} = 0.766$ pF, $L_{rs1} = 69$ nH, $C_{rs1} = 11.13$ pF, $L_{r1} = 13.76$ nH, $C_{r1} = 0.436$ pF, $L_{via} = 80$ nH, $C_d = 1.24$ pF, $L_d = 1.35$ nH. It is obvious from Fig. 11 that the equivalent circuit diagram can realize the dual-band filter with good selectivity at 3.5 GHz and 5.2 GHz, respectively.

After performing optimization analysis on Fig. 11(a) and conducting modeling using HFSS, the simulation results for the parameters S_{11} and S_{21} are shown in Fig. 11(b). The results indicate that the filter exhibits a maximum insertion loss of 0.95 dB and operates at center frequencies of 3.5 GHz and 5.2 GHz, demonstrating a broad range of practical application value. Furthermore, the size of the dual-band filter remains

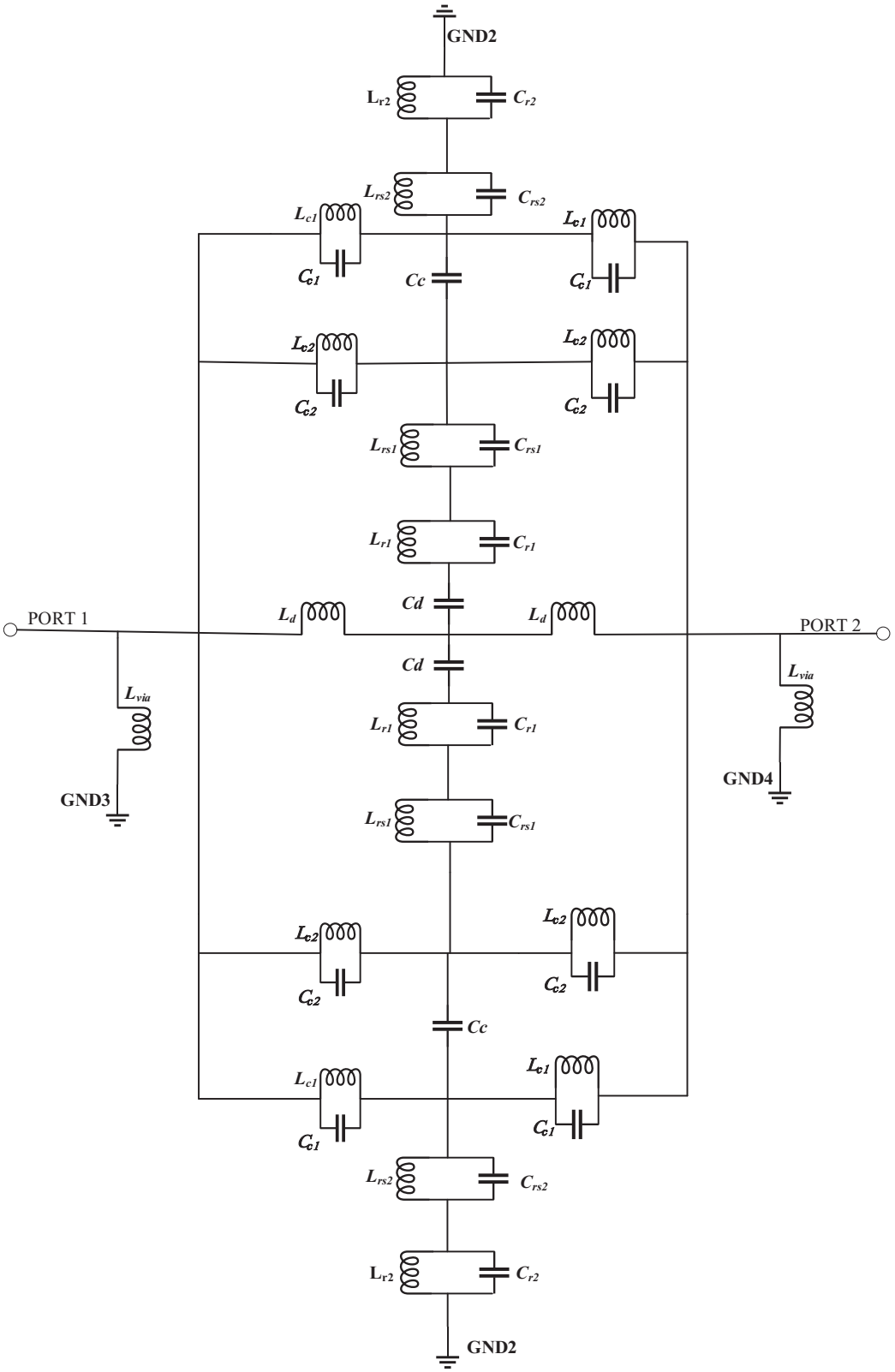

FIGURE 10. Equivalent circuit diagram of SIW loaded symmetric H-type CSRR structure.

largely unchanged compared to the single-band filter, thereby achieving the desired miniaturization performance.

It is noteworthy that by changing the coupling distance b_1 (see Fig. 9), the characteristics related to f_2 can be altered, while f_1 remains unchanged. As the value of b_1 increases, the resonance frequency point of the filter shifts towards lower frequencies. Similarly, the parameter L_4 can also adjust f_2 towards lower frequencies while keeping the frequency response

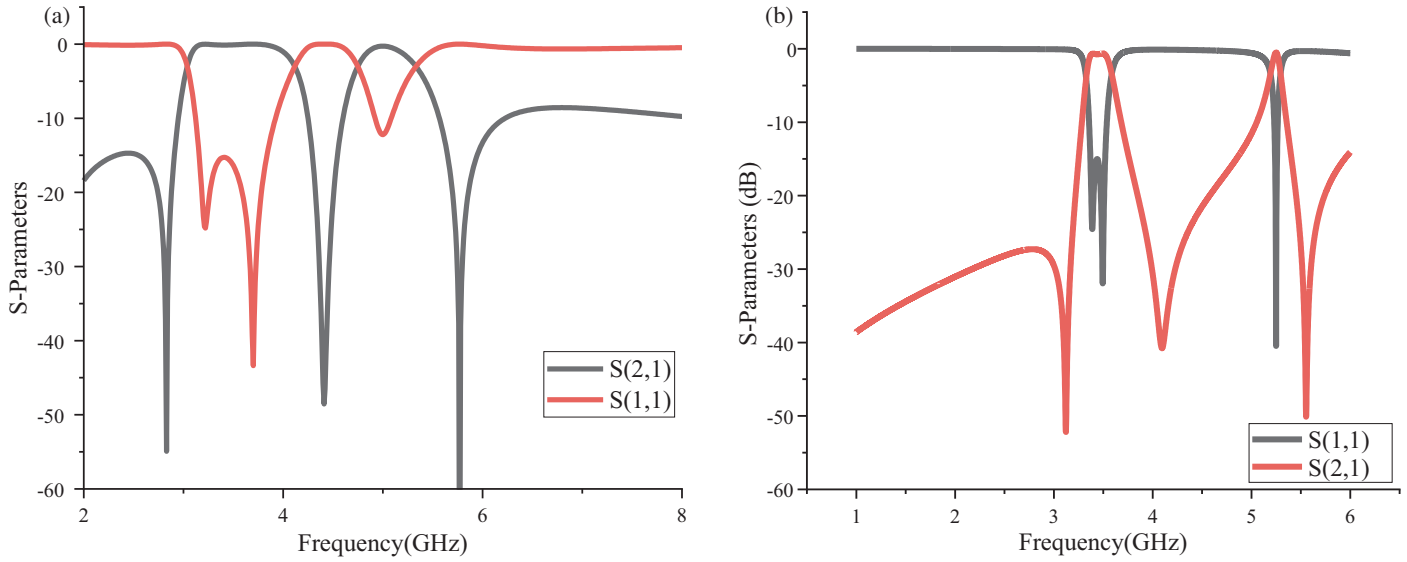

FIGURE 11. (a) Simulation results of equivalent circuit diagram. (b) Parametric simulation results of the dual-band filter.

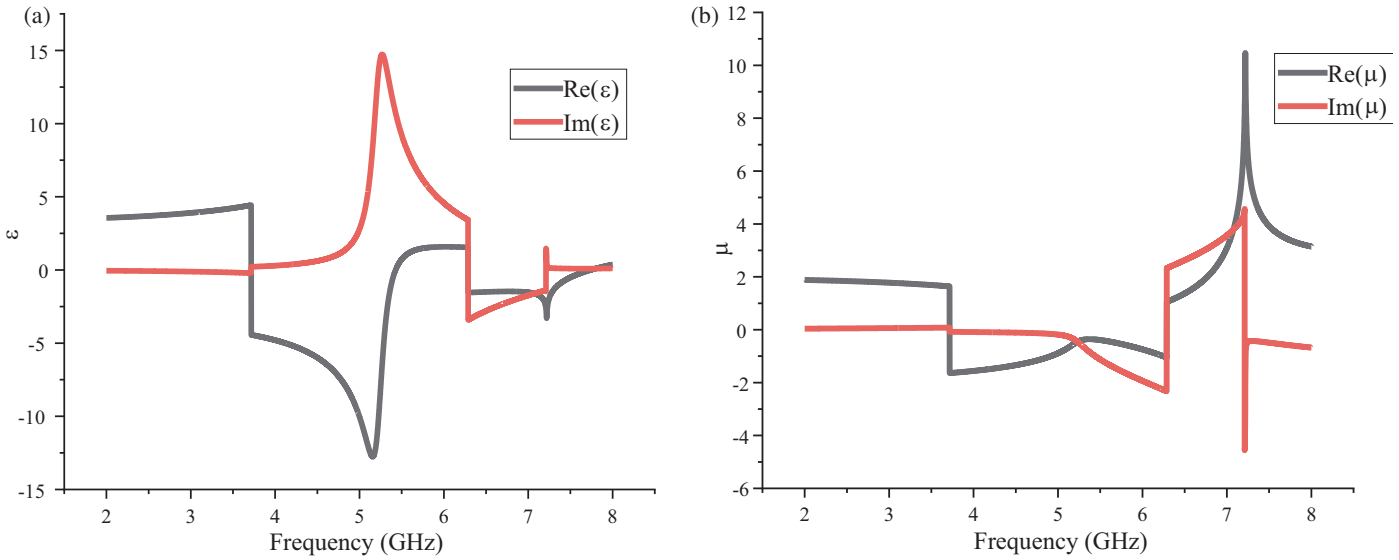

FIGURE 12. Permittivity of SIW loaded H-type CSRR structure and magnetic permeability. (ε is the permittivity and μ is the permeability).

of f_1 unchanged as L_4 increases. Therefore, by modifying the influence of these two parameters, f_2 can be tuned to the desired frequency range. To validate our theory, we will next shift f_2 from 5.2 GHz to 4.8 GHz.

To verify whether the structure exhibits negative permittivity and negative permeability within its passband, this paper applies S-parameter inversion extraction [14]. In this method, the desired permittivity and permeability values are derived through impedance and negative refractive index inversion. The equations for this process are expressed as follows:

$$Z = \pm\sqrt{\frac{(1+S_{11})^2 - S_{21}^2)}{(1-S_{11})^2 - S_{21}^2}}, \tag{5}$$

$$n = \frac{1}{Kd}\left[\left\{\left[In(\frac{S_{21}}{1-S_{11}\frac{Z-1}{Z+1}})\right] + 2\mathrm{m}\pi\right\} -i\left[In(\frac{S_{21}}{1-S_{11}\frac{Z-1}{Z+1}})\right]\right], \tag{6}$$

$$\varepsilon = n/z, \quad \mu = nz, \tag{7}$$

where $K = \varpi_0/c$, m is attributed to the periodicity of the sine function.

In this paper, MATLAB software is utilized to verify the presence of left-handed characteristics, as shown in Fig. 12. The results clearly indicate that both permittivity and permeability are negative within the frequency range of 3.5 GHz to 4.9 GHz. This confirms that the designed dual-band filter exhibits left-handed transmission characteristics.

Based on the simulation results of the dual-band SIW filter in Fig. 11(b), it is evident that the filter exhibits good in-band insertion loss and high selectivity. However, its out-of-band sup-

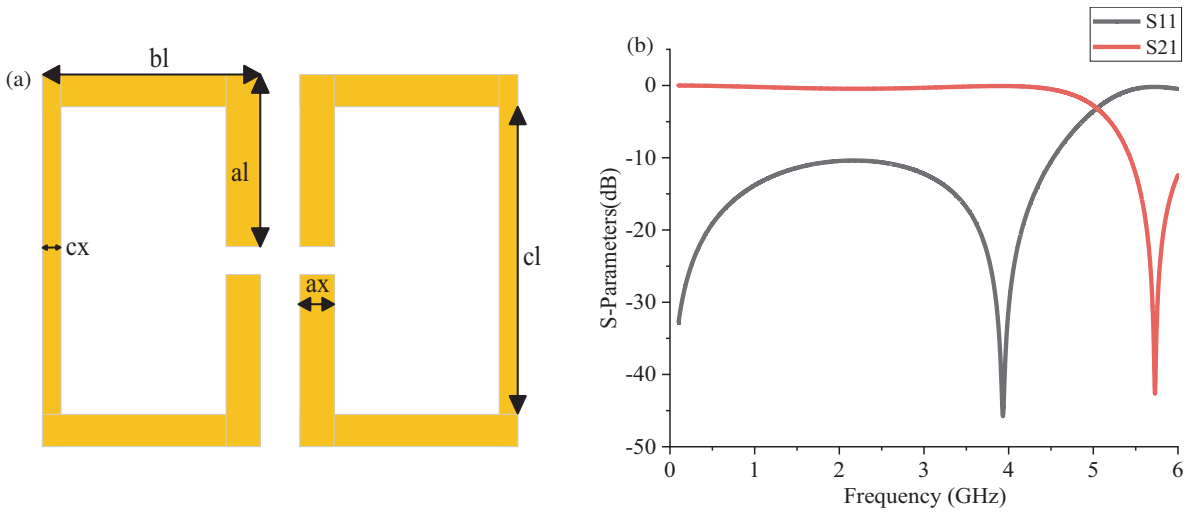

FIGURE 13. (a) The double split-ring resonator DGS structure and its equivalent circuit. (b) The transmission characteristic curve of the double split-ring resonator DGS structure.

TABLE 1. Comparison of various BPF. (IL refers to insertion loss, CRR refers to circular ring resonator.)

Reference	f_0 (GHz)	IL (dB)	Methods	Size ($\lambda_g \times \lambda_g$)
[16]	3.5	1.6	SIR	0.4×0.35
[17]	5.2	2.2	Stub	2.23×1.28
[18]	2.4/5.2	1.4/1.76	Coupling	0.21×0.35
[19]	3.5/5.8	1/1.6	CRR	0.5×0.5
This Work (Single-band)	3.5	0.77	CRLH	0.28×0.18
This Work (Dual-band)	3.5/5.2	0.95/0.56	CRLH	0.28×0.18

pression performance needs improvement. To optimize this, we introduced a defected ground structure (DGS). Compared to a regular transmission line circuit, a microstrip circuit with DGS has a larger electrical length and a lower resonant frequency. Therefore, by reducing the physical length of the transmission line to raise the resonant frequency, it can meet engineering design requirements. This allows for impedance matching while optimizing the circuit size, achieving miniaturization of the device. DGS has the characteristic of a single-pole low-pass filter, and by integrating a DGS structure during the filter design process, it helps suppress higher-order harmonics caused by various factors, thereby improving the out-of-band suppression performance of the filter. In this paper, a dual-symmetric C-shaped DGS structure is etched on the back of the filter in Fig. 4, as shown in Fig. 13(a). The transmission characteristics of the DGS can be seen in Fig. 13(b), where it demonstrates the aforementioned single-pole low-pass characteristics.

From Fig. 14, it can be seen that compared to Fig. 11(b) results, the out-of-band suppression performance has been significantly improved. The filter exhibits high selectivity with center frequencies at 3.5 GHz and 4.9 GHz, operating in the Sub-6G band. The in-band insertion loss is 0.88 dB, and the return loss is less than -15 dB. The model's design size is $0.28\lambda_g \times 0.18\lambda_g$. All these indicators demonstrate that this dual-band SIW filter not only has a compact size but also exhibits excellent in-band performance.

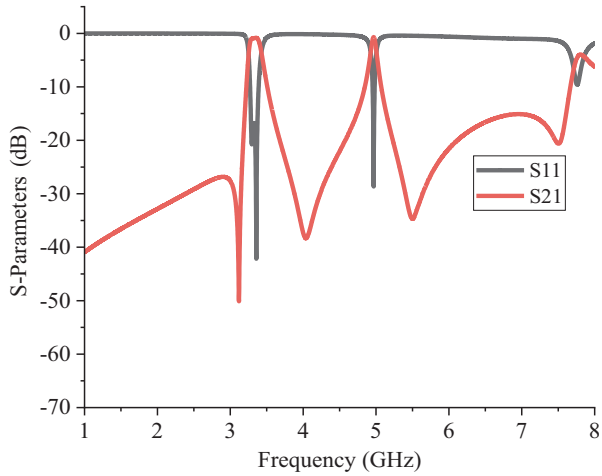

FIGURE 14. The S-parameter simulation results of the SIW dual-band filter.

2.3. Design of a Miniaturized Dual-Band Filter Based on HMSIW

Hong et al. proposed an HMSIW structure [15], noting that HMSIW is formed by cutting a SIW into two semi-open structures (8) using equivalent magnetic walls. Because the width of the SIW is much greater than its height, the electric field distribution after the cut remains almost unchanged. Furthermore, the out-of-band rejection performance of HMSIW is superior

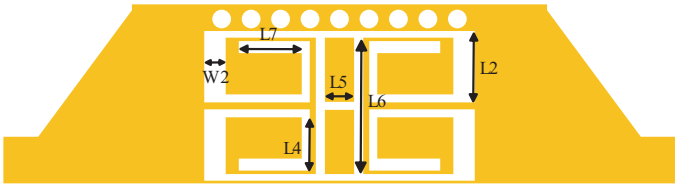

FIGURE 15. Top layer structure of the HMSIW dual-band filter. $L_2 = 2.68\,\text{mm}$, $W_2 = 0.82\,\text{mm}$, $L_7 = 2.35\,\text{mm}$, $L_5 = 1.09\,\text{mm}$, $L_6 = 5.12\,\text{mm}$, $L_4 = 1.7\,\text{mm}$.

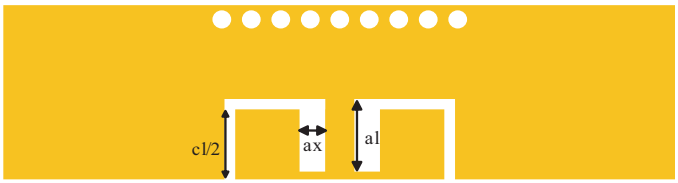

FIGURE 16. Bottom-layer structure of the HMSIW dual-band filter.

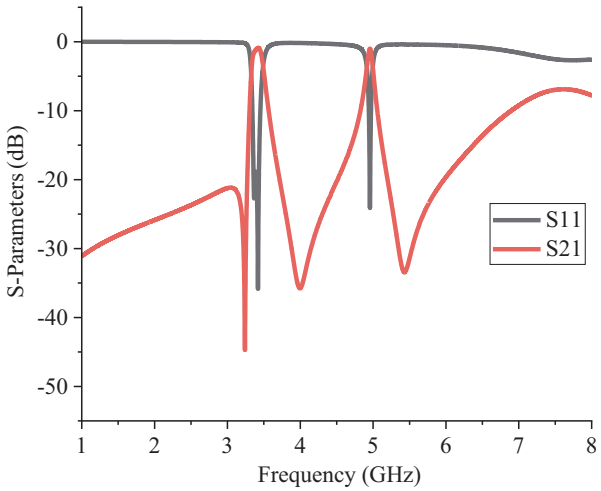

FIGURE 17. Simulation results of the HMSIW dual-band filter.

to that of SIW.

$$f_{c,TE_{0.5,0}} = \frac{c}{4\sqrt{\varepsilon_r} W_{eff,HMSIW}}, \tag{8}$$

where $W_{eff,HMSIW}$ represents the equivalent width of HMSIW.

$$W_{eff,SIW} = 2W_{SIW} - 1.08\frac{d^2}{p} + 0.1\frac{d^2}{2W_{SIW}}, \tag{9}$$

$$W_{eff,HMSIW} = \frac{W_{eff,SIW}}{2} + \Delta W, \tag{10}$$

$$\frac{\Delta W}{h} = \left(0.05 + \frac{30}{\varepsilon_r}\right) \ln\left(0.79\frac{W_{eff,SIW}/2}{h^3} + \frac{(104W_{eff,SIW}/2) - 216}{h^2} + \frac{38}{h} + 2.77\right) \tag{11}$$

The actual dimensions of HMSIW can be calculated using (9), (10), and (11).

By applying the HMSIW principle, the equivalent magnetic wall is cut along the SIW, thereby reducing the filter size without altering the overall filtering performance. The structural model of the dual-band filter based on HMSIW is shown in Fig. 15 and Fig. 16. The S-parameter simulation results of the SIW dual-band filter in Fig. 14 and the HMSIW dual-band filter in Fig. 17 are highly consistent.

3. MEASUREMENT AND ANALYSIS

3.1. Experimental Measurement of the SIW Single-Frequency and Dual-Band Filter

Based on the above analysis, the proposed single-frequency and dual-frequency filters were fabricated and tested. Fig. 18 presents the proposed loaded single H-shaped CSRR filter, while Fig. 19 compares the simulated and measured results. This comparison indicates a general consistency between the simulated and experimental outcomes. Fig. 20 illustrates the proposed dual-frequency filter, and Fig. 21 provides a comparison of its simulated and measured results, showing a high degree of agreement. Minor measurement discrepancies can be attributed to parasitic effects caused by welding and SMA connections. Overall, the designed filters exhibit key characteristics such as miniaturization, low insertion loss, and high selectivity. Table 1 compares the proposed filter with models developed in recent years, highlighting the advantages of the proposed design.

3.2. Experimental Measurement of the HMSIW Dual-Frequency Filter

The HMSIW dual-frequency filter was fabricated and simulated, with the physical structure shown in Fig. 22. As seen in Fig. 22 (a), the designed HMSIW structure reduces the size by approximately 50% compared to the SIW dual-frequency filter, achieving miniaturization. Figs. 22(b) and (c) display

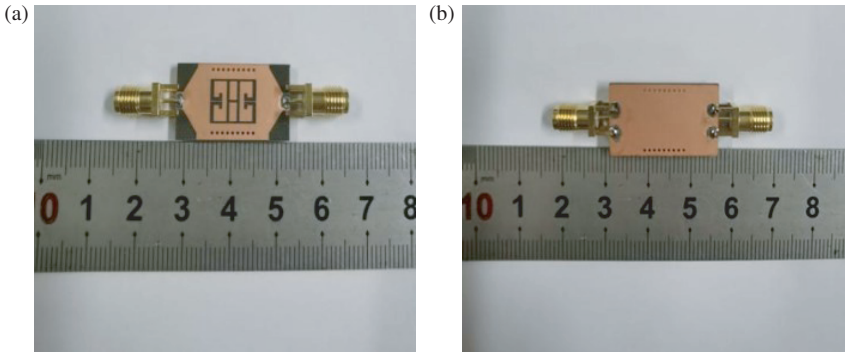

FIGURE 18. (a) The front processing of single-frequency filter. (b) The back processing of single-frequency filter.

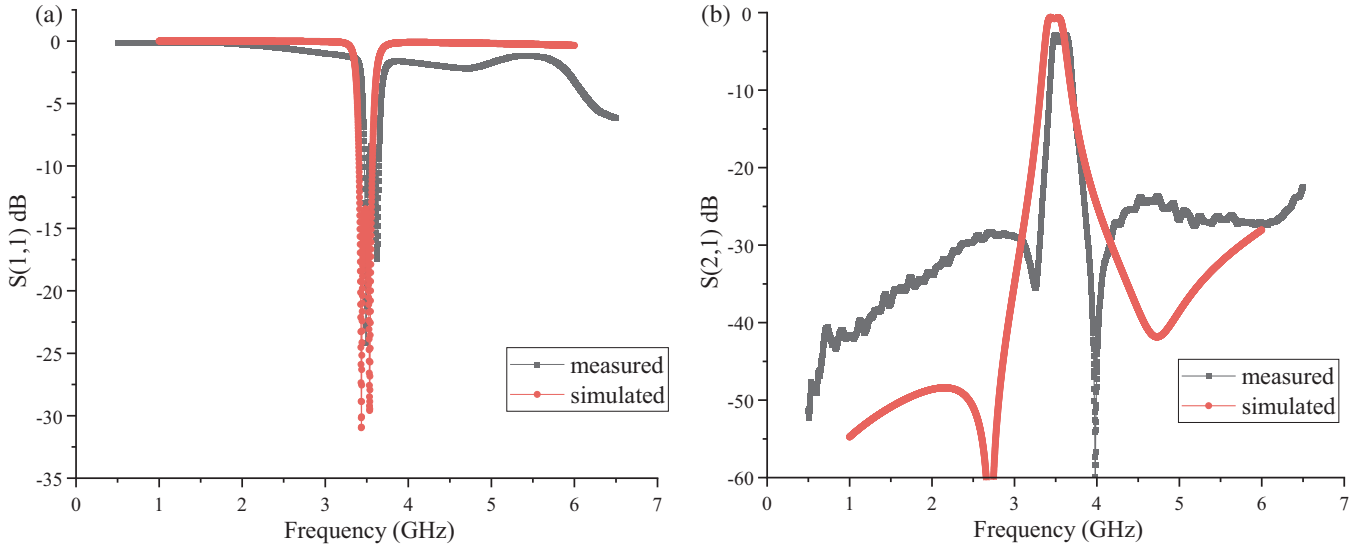

FIGURE 19. (a) Comparison of simulated and measured results of single-frequency filter S_{11}. (b) Comparison of simulated and measured results of single-frequency filter S_{21}.

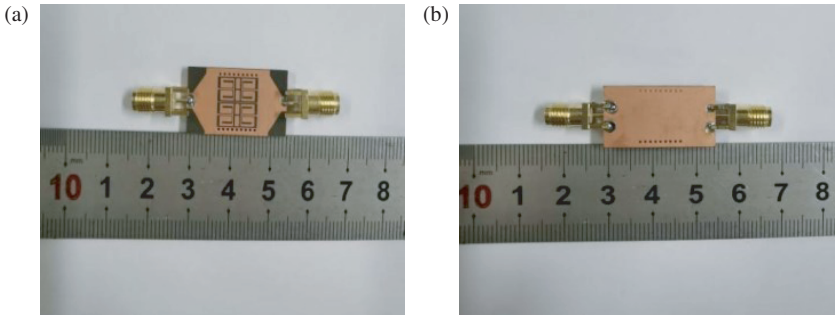

FIGURE 20. (a) The front processing of dual-frequency filter. (b) The back processing of dual-frequency filter.

the front and back structures of the HMSIW filter, respectively, with a comparison of the simulated and measured results shown in Fig. 23.

From the comparison curves of simulated and experimental results in Fig. 23, it can be seen that the measured results are generally consistent with the simulation ones. The resonance frequency and bandwidth closely match the simulated data. The filter operates in the 3.45/4.8 GHz bands, with insertion losses of 1.7 dB and 2.1 dB, respectively, demonstrating good selectivity and miniaturization. A performance comparison with other papers is shown in Table 2.

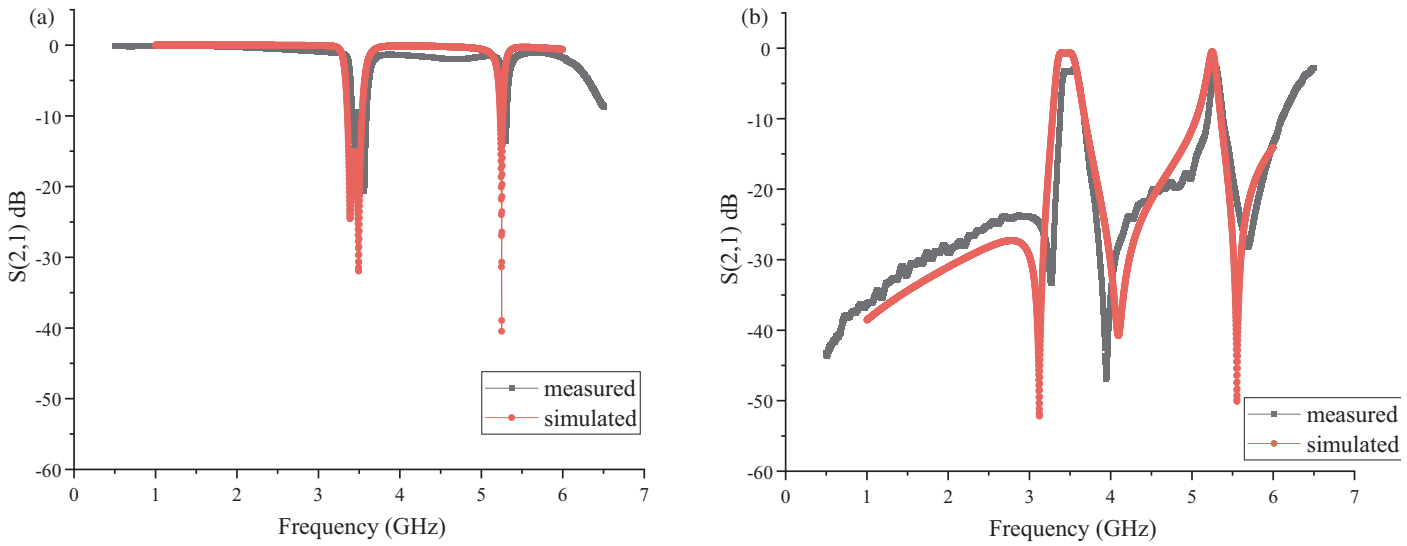

FIGURE 21. (a) Comparison of simulated and measured results of dual-frequency filter S_{11}. (b) Comparison of simulated and measured results of dual-frequency filter S_{21}.

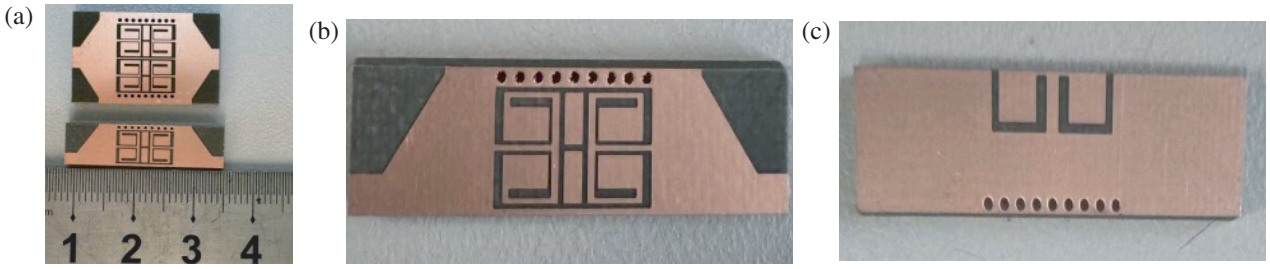

FIGURE 22. Diagram of the HMSIW filter structure and a comparison with the SIW filter structure. (a) Structural comparison. (b) Front structure. (c) Back structure.

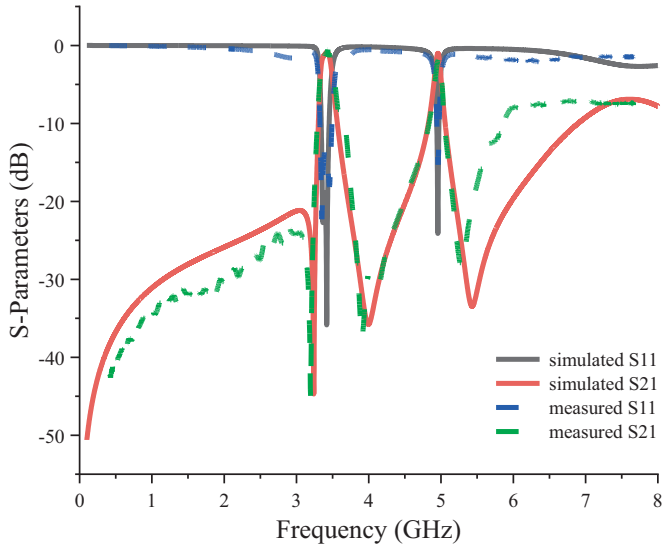

FIGURE 23. Comparison of simulated and measured S-parameters of HMSIW filter.

TABLE 2. Comparison of filter performance with that in the references.

Reference	f_0 (GHz)	IL (dB)	Return Loss	Size ($\lambda_g \times \lambda_g$)
[20]	1.75/3.64	2.0/1.1	18/20	0.27×0.14
[21]	2.46/5.65	1.2/1.9	32/19	0.32×0.15
[22]	3.5/5.24	1.52/1.65	17/18	1.23×1.23
[23]	2.6/5.8	1.1/2.15	35/35	0.34×0.26
This Work	3.45/4.74	1.7/2.1	22/24	0.30×0.08

4. CONCLUSION

This paper demonstrates a dual-band filter with left-handed characteristics, featuring miniaturization, wide bandwidth, high performance, and low loss. The study shows that by introducing symmetric H-shaped CSRR and DGS, left-handed characteristics of the filter and high out-of-band rejection capability were successfully achieved. The incorporation of the HMSIW structure theory further reduces the filter size by 50%. The measured results align well with the simulated ones, validating the effectiveness of the design.

ACKNOWLEDGEMENT

This work was supported in part by Anhui Province Higher Education Science Research Project under Grant 2022AH050070 and in part by the National Natural Science Foundation of China under Grant 62371002.

REFERENCES

[1] Veselago, V. G., "The electrodynamics of substances with simultaneously negative values of ε and μ," *Usp. Fiz. Nauk*, Vol. 92, No. 3, 517–526, 1967.

[2] Pendry, J. B., A. J. Holden, D. J. Robbins, and W. J. Stewart, "Magnetism from conductors and enhanced nonlinear phenomena," *IEEE Transactions on Microwave Theory and Techniques*, Vol. 47, No. 11, 2075–2084, Nov. 1999.

[3] Shelby, R. A., D. R. Smith, and S. Schultz, "Experimental verification of a negative index of refraction," *Science*, Vol. 292, No. 5514, 77–79, 2001.

[4] Falcone, F., T. Lopetegi, J. D. Baena, R. Marques, F. Martin, and M. Sorolla, "Effective negative-/spl epsiv/stopband microstrip lines based on complementary split ring resonators," *IEEE Microwave and Wireless Components Letters*, Vol. 14, No. 6, 280–282, Jun. 2004.

[5] Che, W., C. Li, K. Deng, and L. Yang, "A novel bandpass filter based on complementary split rings resonators and substrate integrated waveguide," *Microwave and Optical Technology Letters*, Vol. 50, No. 3, 699–701, Mar. 2008.

[6] Choudhary, D. K. and R. K. Chaudhary, "A compact SIW based filtering power divider with improved selectivity using CSRR," in *2017 Progress in Electromagnetics Research Symposium - Fall (PIERS - FALL)*, 1334–1337, Singapore, 2017.

[7] Liu, Z., G. Xiao, and L. Zhu, "Triple-mode bandpass filters on CSRR-loaded substrate integrated waveguide cavities," *IEEE Transactions on Components, Packaging and Manufacturing Technology*, Vol. 6, No. 7, 1099–1105, Jul. 2016.

[8] Dong, Y. and T. Itoh, "Miniaturized dual-band substrate integrated waveguide filters using complementary split-ring resonators," in *2011 IEEE MTT-S International Microwave Symposium*, 1–4, Baltimore, MD, USA, 2011.

[9] Zhang, Q.-L., W.-Y. Yin, S. He, and L.-S. Wu, "Compact substrate integrated waveguide (SIW) bandpass filter with complementary split-ring resonators (CSRRs)," *IEEE Microwave and Wireless Components Letters*, Vol. 20, No. 8, 426–428, Aug. 2010.

[10] Zhang, S., J.-Y. Rao, J.-S. Hong, and F.-L. Liu, "A novel dual-band controllable bandpass filter based on fan-shaped substrate integrated waveguide," *IEEE Microwave and Wireless Components Letters*, Vol. 28, No. 4, 308–310, Apr. 2018.

[11] Urick, V. J., F. Bucholtz, P. S. Devgan, J. D. McKinney, and K. J. Williams, "Phase modulation with interferometric detection as an alternative to intensity modulation with direct detection for analog-photonic links," *IEEE Transactions on Microwave Theory and Techniques*, Vol. 55, No. 9, 1978–1985, Sep. 2007.

[12] Touiss, T., M. R. Qasem, S. Machichi, F. Falyouni, and D. Bria, "New THz notch filter based on cylindrical periodic structure," *Progress In Electromagnetics Research Letters*, Vol. 121, 51–56, 2024.

[13] Bozzi, M., A. Georgiadis, and K. Wu, "Review of substrate-integrated waveguide circuits and antennas," *IET Microwaves, Antennas & Propagation*, Vol. 5, No. 8, 909–920, 2011.

[14] Numan, A. B. and M. S. Sharawi, "Extraction of material parameters for metamaterials using a full-wave simulator [education column]," *IEEE Antennas and Propagation Magazine*, Vol. 55, No. 5, 202–211, 2013.

[15] Hong, W., B. Liu, Y. Wang, Q. Lai, H. Tang, X. X. Yin, Y. D. Dong, Y. Zhang, and K. Wu, "Half mode substrate integrated waveguide: A new guided wave structure for microwave and millimeter wave application," in *2006 Joint 31st International Conference on Infrared Millimeter Waves and 14th International Conference on Teraherz Electronics*, 219–219, Shanghai, China, 2006.

[16] Zhang, M., M. Li, P. J. Zhang, K. Duan, B. Jin, L. Huang, and Y. Song, "A novel miniaturized bandpass filter basing on stepped-impedance resonator," *Progress In Electromagnetics Research Letters*, Vol. 97, 77–85, 2021.

[17] Riaz, L., U. Naeem, and M. F. Shafique, "Miniaturization of SIW cavity filters through stub loading," *IEEE Microwave and Wireless Components Letters*, Vol. 26, No. 12, 981–983, Dec. 2016.

[18] Yan, J.-M., L.-Z. Cao, J. Xu, and R.-S. Chen, "Design of a fourth-order dual-band bandpass filter with independently controlled external and inter-resonator coupling," *IEEE Microwave and Wireless Components Letters*, Vol. 25, No. 10, 642–644, Oct. 2015.

[19] Li, D., Y. Zhang, K. Xu, K. Song, and L.-W. Li, "Dual-band bandpass filter with good selectivity and stopband rejection," in *PIERS Proceedings*, 582–586, Guangzhou, China, 2014.

[20] Tang, J., H. Liu, and Y. Yang, "Compact wide-stopband dual-band balanced filter using an electromagnetically coupled SIR pair with controllable transmission zeros and bandwidths," *IEEE Transactions on Circuits and Systems II: Express Briefs*, Vol. 67, No. 11, 2357–2361, Nov. 2020.

[21] Zhou, L.-H. and J.-X. Chen, "Differential dual-band filters with flexible frequency ratio using asymmetrical shunt branches for wideband CM suppression," *IEEE Transactions on Microwave Theory and Techniques*, Vol. 65, No. 11, 4606–4615, Nov. 2017.

[22] Li, P., H. Chu, D. Zhao, and R. S. Chen, "Compact dual-band balanced SIW bandpass filter with improved common-mode suppression," *IEEE Microwave and Wireless Components Letters*, Vol. 27, No. 4, 347–349, Apr. 2017.

[23] Ren, B., H. Liu, Z. Ma, M. Ohira, P. Wen, X. Wang, and X. Guan, "Compact dual-band differential bandpass filter using quadruple-mode stepped-impedance square ring loaded resonators," *IEEE Access*, Vol. 6, 21 850–21 858, 2018.